Targeted Iron-Oxide Nanoparticle for Photodynamic Therapy and Imaging of Head and Neck Cancer

Dongsheng Wang,[†] Baowei Fei,[‡,#,*] Luma V. Halig,[‡] Xulei Qin,[#] Zhongliang Hu,[†] Hong Xu,[⊥] Yongqiang Andrew Wang,[⊥] Zhengjia Chen,[§,||] Sungjin Kim,[||] Dong M. Shin,[†] and Zhuo (Georgia) Chen[†,*]

[†]Department of Hematology and Medical Oncology, Winship Cancer Institute, [‡]Department of Radiology and Imaging Sciences, and [§]Department of Biostatistics and Bioinformatics, Emory University School of Medicine, Atlanta, Georgia 30322, United States, [⊥]Ocean NanoTech LLC, San Diego, California 92126, United States, [||]Biostatistics and Bioinformatics Shared Resource at Winship Cancer Institute, Emory University, Atlanta, Georgia 30322, United States, and [#]Department of Biomedical Engineering, Emory University and Georgia Institute of Technology, Atlanta, Georgia 30322, United States

ABSTRACT Photodynamic therapy (PDT) is a highly specific anticancer treatment modality for various cancers, particularly for recurrent cancers that no longer respond to conventional anticancer therapies. PDT has been under development for decades, but light-associated toxicity limits its clinical applications. To reduce the toxicity of PDT, we recently developed a targeted nanoparticle (NP) platform that combines a second-generation PDT drug, Pc 4, with a cancer targeting ligand, and iron oxide (IO) NPs. Carboxyl functionalized IO NPs were first conjugated with a fibronectin-mimetic peptide (Fmp), which binds integrin β1. Then the PDT drug Pc 4 was successfully encapsulated into the ligand-conjugated IO NPs to generate Fmp-IO-Pc 4. Our study indicated that both nontargeted IO-Pc 4 and targeted Fmp-IO-Pc 4 NPs accumulated in xenograft tumors with higher concentrations than nonformulated Pc 4. As expected, both IO-Pc 4 and Fmp-IO-Pc 4 reduced the size of HNSCC xenograft tumors more effectively than free Pc 4. Using a 10-fold lower dose of Pc 4 than that reported in the literature, the targeted Fmp-IO-Pc 4 NPs demonstrated significantly greater inhibition of tumor growth than nontargeted IO-Pc 4 NPs. These results suggest that the delivery of a PDT agent Pc 4 by IO NPs can enhance treatment efficacy and reduce PDT drug dose. The targeted IO-Pc 4 NPs have great potential to serve as both a magnetic resonance imaging (MRI) agent and PDT drug in the clinic.
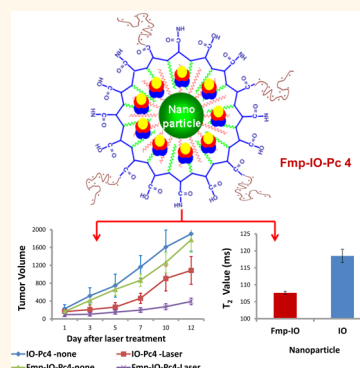
KEYWORDS: iron-oxide nanoparticle · Fmp-IO-Pc 4 · photodynamic therapy · head and neck cancer · magnetic resonance imaging · integrin β1

Head and neck cancer accounted for an estimated 53 640 new cases and 11 520 deaths in the US in 2013.[1] It is one of the most common cancers and is responsible for almost 200 000 deaths around the world every year.[2] About 33—50% of patients with head and neck squamous cell carcinoma (HNSCC) develop locoregional recurrence, which is a major factor contributing to poor prognosis and quality of life.[3] For many of these patients, surgery and radiation therapy approaches have been exhausted, and conventional chemotherapy is the remaining option but with limited efficacy and often intolerable toxicity. Nonspecific distribution, which results in insufficient drug accumulation in the tumor, off-target attack of normal cells, and unacceptable toxicity are the major limitations of current chemotherapeutic agents.[4]

New therapeutic strategies that feature targeted drug delivery and low side effects are much needed for the treatment of HNSCC.

Photodynamic therapy (PDT) is increasingly being recognized as an attractive alternative treatment for various cancers.[5,6] It involves the activation of a photosensitizer (PS) with light of specific wavelength, which interacts with molecular oxygen to generate singlet oxygen and other reactive oxygen species (ROS), leading to tumor cell death through apoptosis and necrosis.[7] PDT has proven to be effective in combination with other therapeutic modalities, such as surgery, chemotherapy, and radiotherapy.[8,9] It is a promising alternative for superficial malignant or premalignant lesions of the head and neck.[10—13] PDT has also proven useful for those with recurrent surface disease after surgery or radiotherapy.[11] Silicon phthalocyanine

photosensitizer Pc 4 [HOSiPcOSi(CH$_3$)$_2$(CH$_2$)$_3$N-(CH$_3$)$_2$] is a new generation of photosensitizer.[14] It has been shown to be effective in the treatment various types of cancer in animal models.[15−22] In addition, several clinical trials have been carried out to examine the clinical applicability of this photosensitizer.[15]

Early clinical results suggest nanoparticle (NP)-based therapeutics for cancer show enhanced efficacy and reduced side effects as a result of their properties such as targeted localization in tumors and active cellular uptake.[23] In the past decade, nanocarriers have changed the landscape of healthcare drastically, particularly in several areas of diagnosis and drug delivery. Among the various types of nanocarriers that have been explored for drug delivery, iron-oxide nanoparticles (IO) have shown particular promise in magnetic resonance imaging (MRI) in diagnostic radiology.[24−26] IO NPs have significant advantages as biomedicines because they are biocompatible and nontoxic to humans[27] and accordingly have been approved as an MRI contrast agent by the U.S. Food and Drug Administration (FDA).[28,29] Therefore, IO NPs have the potential to serve as both nanocarrier and imaging agent.

To enhance the accumulation of IO NPs in HNSCC tissues, we selected integrin β1 as a target for the targeted delivery of IO NPs. Association of integrin β1 with HNSCC has been reported in several studies.[30,31] Eke et al. demonstrated integrin β1 is essential for head and neck cancer resistance to radiotherapy.[32] Our own study has recently shown that integrin β1 expression is higher in metastatic than nonmetastatic HNSCC and plays a major role in HNSCC metastasis.[33] These previous studies suggest integrin β1 could be an appropriate target for head and neck cancer therapy. Fibronectin mimetic peptide (Fmp) has been shown to effectively bind to integrin β1 in vivo and be useful as a ligand for targeted therapy.[34,35] In the current study, we have developed an integrin β1-mediated targeted PDT nanomedicine, which has the potential to be used to treat localized tumors such as residual or recurrent HNSCC of the oral cavity, pharynx, larynx, and derma and with reduced side effects.

RESULTS

Synthesis and Characterization of IO Nanoparticles. Fmp was conjugated to carboxyl functionalized IO NPs with diameter of 10 nm in a molar ratio of 30:1. The molar ratio of Fmp to IO NPs was 27:1 in the final product since the conjugation efficiency of Fmp was 89.5% as determined by HPLC analysis (Supporting Information, Figure S1). For drug loading, 1 mg of Pc 4 dissolved in methanol (1 mg/mL) was added to 1 mg of Fmp-IO (1 mg (Fe)/ml). The loading was confirmed by running the mixture through a spin column (MWCO: 10K) to check the color of flow through. On the basis of the molar extinction coefficient of Pc 4 (668 nm, 230 000) and 10 nm IO NPs (500 nm, 4 700 000), each IO NP

contains an estimated 142.6 molecules of Pc 4. Figure 1A shows a schematic illustration of the synthesis of water-soluble Fmp-IO-Pc 4. As shown by TEM imaging in Figure 1B, the IO NPs are highly uniform with an average size of 10 nm. The hydrodynamic size of Fmp-IO-Pc 4 is 41 nm measured by dynamic light scattering (DLS). Figure 1C shows size-dependent migrations of the different sized IO, Fmp-IO and Fmp-IO-Pc 4 in 2% agarose gel. Since Fmp-IO-Pc 4 has the largest molecular weight and size, it migrated with the slowest speed in the gel. Absorption spectra showed that the synthesized Fmp-IO-Pc 4 (purple) has a similar specific absorption at around 675 nm as the free Pc 4 (blue) (Figure 1D).

***In Vitro* Efficacy of Fmp-IO-Pc 4 in HNSCC Cell Lines.** To verify the bioactivity of nanoparticlized Pc 4, four HNSCC cell lines M4E, M4E-15, 686LN, and TU212 were exposed to Pc 4, IO-Pc 4 and Fmp-IO-Pc 4 at the same concentrations of Pc 4. M4E-15 is an integrin β1 knock-down derivative of the M4E cell line isolated after integrin β1-specific shRNA transfection.[33] Laser treatment was given after 24 h of drug administration. Sulforhodamine B (SRB) assay was performed 24 and 48 h later to evaluate the efficacy of newly synthesized nanoparticle drugs. As shown in Figure 2, both Fmp-IO-Pc 4 and IO-Pc 4 had equal efficacy as free Pc 4 in the SRB study, indicating that conjugated Pc 4 in IO NPs is as biologically active as free Pc4. There were no significant differences in the sensitivity of these cell lines to Pc 4 PDT in vitro. This observation was confirmed by singlet oxygen measurement after laser activation of Pc 4, IO-Pc 4, and Fmp-IO-Pc 4 in aqueous conditions (pH 7.0) using singlet oxygen sensor green (SOSG).[36] Similar amounts of singlet oxygen were generated by the three agents under equivalent Pc 4 concentrations, indicating that Pc 4 activity is not affected by its encapsulation into IO NPs (data not shown).

Preferential Binding of Fmp-IO-Pc 4 to Integrin β1 Positive Cells. To evaluate the specificity of Fmp targeting to HNSCC cells, we conducted an in vitro binding assay. M4E control cells and integrin β1 knock-down M4E derivatives (M4E-15) were exposed to IO-Pc 4 and Fmp-IO-Pc 4 for 2 h at 4 and 37 °C. Cells were then washed and fixed. Pc 4 binding was imaged using a Nuance Multispectral Image System Nuance 3.1 (Caliper/PerkinElmer Life Sciences and Technology, Hopkinton, MA). As shown in Figure 3, at 4 °C only Fmp-IO-Pc 4 was able to bind to the M4E control cells that express integrin β1, while IO-Pc4 failed to bind M4E cells (Figure 3A). The imaging result also showed that Fmp-IO-Pc4 was not able to bind to M4E-15 cells whose integrin β1 expression was reduced by integrin β1 specific shRNA. On the other hand, at 37 °C, both IO-Pc 4 and Fmp-IO-Pc 4 showed positive Pc 4 staining in both M4E cells and M4E-15 cells through endocytosis (Figure 3B). Figure 3C and Figure 3D show

A

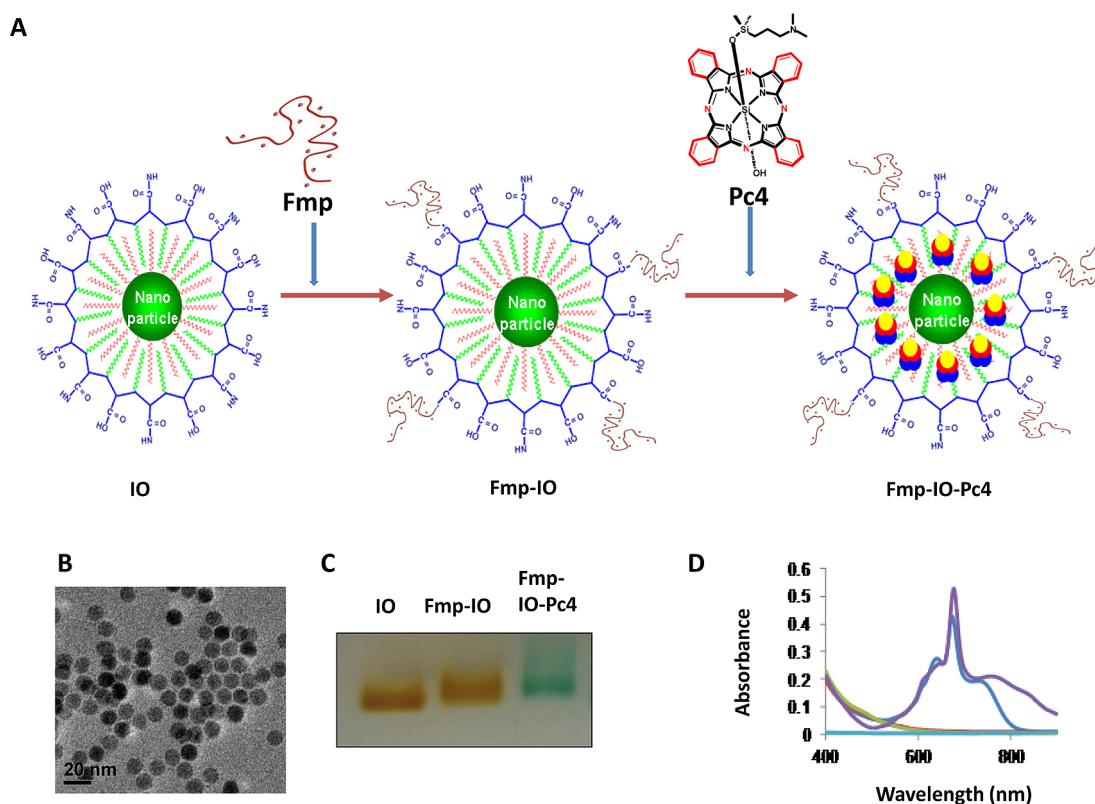IO   Fmp-IO   Fmp-IO-Pc4

B

C

D

Figure 1. Construction of targeted IO nanoparticles carrying Pc 4. (A) Schematic illustration of synthesis of water-soluble Fmp-IO-Pc 4 using Ocean's amphiphilic polymer-coated IO nanoparticles. (B) TEM image of IO NPs, which are highly homogeneous with an average size of 10 nm. (C) Size-dependent migration of different sized IO, Fmp-IO and Fmp-IO-Pc 4 NPs in 2% agarose gel. Since Fmp-IO-Pc 4 has the largest molecular weight and size, it migrated slowest in the gel. (D) The absorption spectra of synthesized Fmp-IO-Pc 4. As shown, Fmp-IO-Pc 4 (purple) has a similar absorption at around 675 nm as the free Pc 4 (blue) while IO (red) and solvent (green) show no specific absorption at 675 nm.

the quantified fluorescence signal of Pc 4 in IO NPs in the indicated cell lines. At 4 °C, the binding signal for Fmp-IO-Pc 4 in M4E cells was significantly higher than that in M4E-15 cells ($p < 0.001$). Furthermore, the binding signal for Fmp-IO-Pc4 in M4E cells was significantly higher than that of IO-Pc 4 ($p < 0.001$) (Figure 3C). The specific binding of Fmp-IO-Pc 4 was further confirmed in M4E and M4E-15 cells at 4 °C and observed by confocal microscopy (Zeiss LSM 510 META system, Carl Zeiss MicroimagingInc., Thornwood NY) (Supporting Information, Figure S2). On the other hand, at 37 °C, Fmp-IO-Pc 4 showed a significantly higher Pc 4 signal than IO-Pc 4 ($p < 0.001$), but there was no significant difference in Fmp-IO-Pc 4 internalization between M4E and M4E-15 cells (Figure 3D).

Efficacy of IO-Pc 4 NPs in an HNSCC Animal Model. In a xenograft tumor animal model study, human HNSCC M4E cells were injected on both sides of each mouse. When tumors reached 5−7 mm in diameter, the mice were randomized into four groups with 6 mice in each group. Each group was given a single equivalent dose of 0.4 mg/kg Pc 4 in the form of free Pc 4, IO-Pc 4, and Fmp-IO-Pc 4 by intravenous (I.V.) injection, accordingly. Mice in the control group were given phosphate-buffered saline (PBS). Laser treatment of the tumors was conducted 48 h after administration of the drugs

on the right side tumors only. Left side tumors remained untreated. Tumor size was measured every 2 days. Figure 4A shows that both targeted (Fmp-IO-Pc 4) and nontargeted (IO-Pc 4) NPs significantly reduced tumor growth compared to the PBS control group ($p < 0.003$ and 0.022, respectively), while free Pc 4 only marginally reduced the tumor size as compared with the PBS control ($p < 0.07$). IO-Pc 4 and Fmp-IO-Pc 4 treated groups had significantly smaller tumor volume than the free Pc 4 group ($p = 0.05$ and 0.04, respectively). To rule out any effect of the IO nanoparticles on tumor growth under laser treatment, since IO may be heated up under laser frequency, we performed the same *in vivo* experiment as described using the same IO concentration as Fmp-IO-Pc 4 (1.35 mg/kg Fe). No significant difference in tumor growth was observed between laser treated and nontreated tumors in the IO group (Supporting Information, Figure S3). There was no significant difference in treatment efficacy between Fmp-IO-Pc 4 and IO-Pc 4 ($p = 0.9$).

To further explore if the targeted Fmp-IO-Pc 4 NPs have any advantage in efficacy over the nontargeted IO-Pc 4 NPs, we administered the mice IO-Pc 4 and Fmp-IO-Pc 4 at a low dose of 0.06 mg/kg Pc 4 equivalent. As shown in Figure 4B, growth of the tumors after laser illumination was significantly slower than without
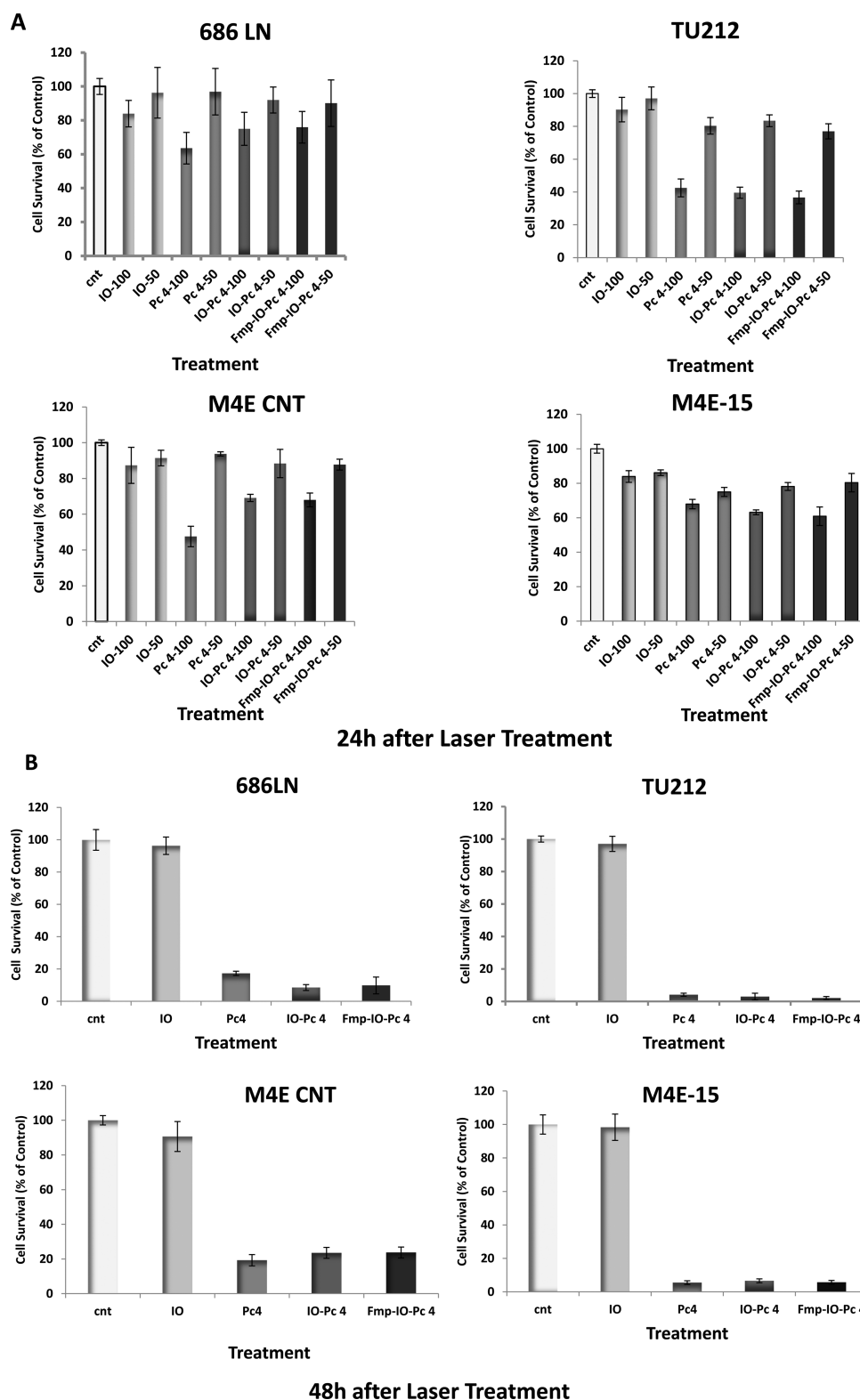
A

686 LN

TU212

M4E CNT

M4E-15

24h after Laser Treatment

B

686LN

TU212

M4E CNT

M4E-15

48h after Laser Treatment

Figure 2. *In vitro* inhibition of HNSCC cell growth. SRB assay shows that both free Pc 4 and NP-based Pc 4 have good drug efficacy in several HNSCC cancer cell lines, M4E, M4E-15, 686LN, and TU212. The cancer cells were grown in medium with 50 nM or 100 nM Pc 4, IO-Pc 4 or Fmp-IO-Pc 4 at equivalent concentrations of Pc 4 for 24 h. Cells were then subjected to laser treatment. SRB assay was performed 24 and 48 h post laser treatment. (A) 24 h after laser treatment, both Fmp-IO-Pc 4 and IO-Pc 4 showed dose dependent efficacy equal to that of free Pc 4. (B) 48 h after laser treatment, all treatments caused death of the majority of cells at the same concentration of 50 nM, indicating that the encapsulated Pc4 in Fmp-IO-Pc 4 or IO-Pc 4 is as biologically active as free Pc 4.

laser in both IO-Pc 4 and Fmp-IO-Pc 4 groups over time ($p < 0.001$ and $p < 0.001$, respectively). Comparing the

laser illuminated groups, the growth of tumors in the Fmp-IO-Pc 4 NPs (targeted) group was significantly
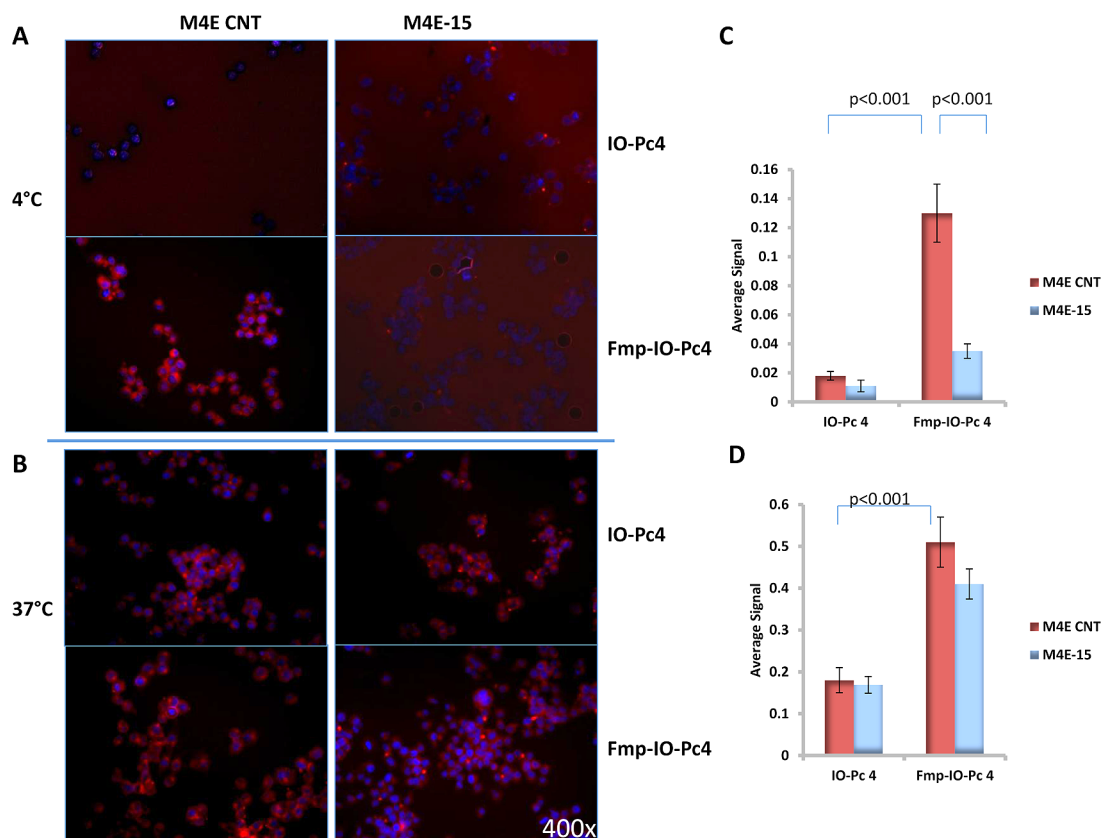
Figure 3. *In vitro* binding assays to compare targeted Fmp-IO-Pc 4 with nontargeted IO-Pc 4 NPs in HNSCC cells. M4E, an integrin β1-positive cell line, and M4E-15, an integrin β1 knock-down derivative of M4E, were seeded on chamber slides at 3000 cells per well. IO-Pc 4 and Fmp-IO-Pc 4 at 100 nM were added 24 h later. Cells were kept at 4 or 37 °C for 2 h. (A) At 4 °C only Fmp-IO-Pc4 bound to integrin β1-positive M4E cells, while very low positive signals were detected for nontargeted IO-Pc4. Very low Fmp-IO-Pc 4 binding was detected in M4E-15 cells. (B) At 37 °C, binding of both Fmp-IO-Pc 4 and IO-Pc 4 was detected to M4E and M4E-15 cells, but Fmp-IO-Pc 4 had a significantly higher signal than IO-Pc 4. Quantified Pc 4 signals on the cells as indicated at 4 °C (C) and 37 °C (D) were obtained using the Nuance Multispectral Image System Nuance 3.1.

slower than that in the IO-Pc 4 NPs (nontargeted) group over time [stratified analysis for laser illumination only with generalized estimating equation (GEE) model, $p < 0.025$].

To explore any potential toxicity of Pc 4, IO-Pc 4, and Fmp-IO-Pc 4 used in the efficacy study at a concentration of 0.4 mg/kg Pc 4, body weights of the mice were recorded, and hematoxylin and eosin (H&E) staining for the major organs was conducted for indications of possible drug toxicity. No body weight loss or tissue damage was observed, indicating no drug related toxicity during these treatments (Supporting Information, Figure S4 and S5).

Comparison of Biodistribution of Fmp-IO-Pc 4 with Free Pc 4 and Nontargeted IO-Pc 4 in HNSCC Xenografted Tumors and Major Organs of Mice. To understand our observation of improved treatment efficacy when using NP-based Pc 4 compared with free Pc 4, the biodistribution of all three drugs was tracked using CRi Maestro imaging system (Caliper/PerkinElmer Life Sciences and Technology, Hopkinton, MA). Mice were given Pc 4, IO-Pc 4, and Fmp-IO-Pc 4 at an equivalent dose of 0.4 mg/kg Pc 4. Both whole-body and organ images of the mice were taken at 4, 24, and 48 h after drug administration.

Figure 5A,B,C shows the fluorescence images and measured signals at different time points in different organs including xenografted tumors from the free Pc 4, IO-Pc 4, and Fmp-IO-Pc 4 groups. Figure 5D shows the Pc 4 signals in whole-body images from Pc 4, IO-Pc 4 and FmP-IO-Pc4-treated groups at different time points. As illustrated, the Pc 4 signals from the targeted NP Fmp-IO-Pc 4 group were slightly higher in tumors than those from the nontargeted NP IO-Pc 4 group at 4 and 48 h after drug injection. Both Fmp-IO-Pc 4 and IO-Pc 4 had significantly higher tumor retention than free Pc 4 ($p < 0.05$ in both cases) at 4, 24, and 48 h. Both IO Pc 4 NPs also showed a higher level of Pc 4 biodistribution in all major organs than free Pc 4 at 4 h, but the Pc 4 level in most of the organs except the skin was largely reduced after 48 h. Meanwhile, after 24 or 48 h, both IO-Pc 4 and Fmp-IO-Pc 4 maintained similar fluorescence signals as free Pc 4 in various organs, indicating that there is no prolonged NP drug retention in major organs compared to free Pc 4.

To examine whether the accumulation of NP-based Pc 4 occurred in tumor cells, tumors were collected and sectioned 24 h after drug injection. The tissue sections were examined for Pc 4 fluorescence signals using
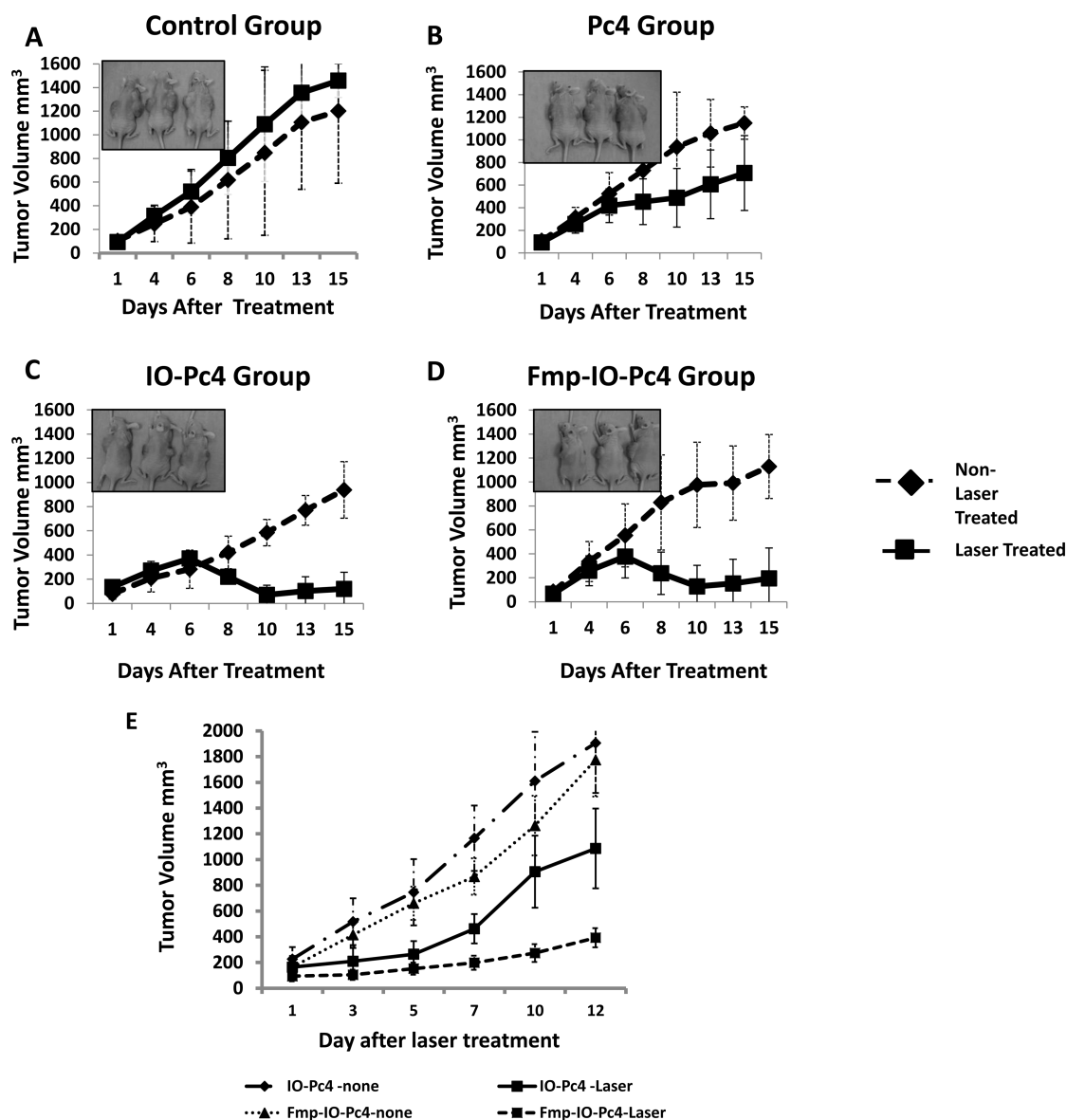
Figure 4. Inhibition of xenograft tumor formation by Pc 4 PDT delivered by IO nanoparticles. (A−D) Tumor growth and representative images of tumors on both sides of the mice in the PBS control, free Pc 4, IO-Pc 4, and Fmp-IO-Pc4 groups, respectively. Pc 4 was given at a concentration of 0.4 mg/kg. Laser treatment was performed 48 h after the drug administration. Three out of six mice from each group are shown as representatives. Statistical analysis indicated a significant difference in the longitudinal tumor volume across the 5 groups within the right side (laser treated), ($p < 0.0013$). Both IO-Pc 4 and Fmp-IO-Pc 4 groups had a significantly lower tumor growth volume than the PBS control group ($p < 0.022$ for IO-Pc 4 and 0.0038 for Fmp-IO-Pc 4). The Pc 4 group had a marginally significantly lower tumor growth volume than the control group ($p < 0.071$). The Pc 4 group had a significantly higher tumor growth volume than both the IO-Pc 4 and Fmp-IO-Pc 4 groups ($p < 0.049$ for IO-Pc 4 group and 0.040 for Fmp-IO-Pc 4 groups). No tumor growth difference was found between IO-Pc 4 and Fmp-IO-Pc 4 groups ($p = 0.98$). There was no significant difference in the longitudinal tumor volume across the 4 groups on the left side tumor (no laser treatment, $p = 0.4987$). None of the pairwise comparisons in tumor volume between any two groups with untreated left tumors was significantly different (results are omitted). **(E)** Tumor growth curve using a lower dose (0.06 mg/kg) and shorter period of time between drug administration and laser treatment than used in (A−D). Tumors in the Fmp-IO-Pc 4 (targeted) group grew significantly slower than those in the IO-Pc 4 group (nontargeted) ($p < 0.025$).

confocal microscopy (Zeiss LSM 510 META system). As shown in Figure 5E, there was more Pc 4 accumulation in the tumor cells from Fmp-IO-Pc4 treated mice than in those from IO-Pc 4 treated mice. Both groups treated with NP-based Pc 4 had greater Pc4 accumulation in tumor tissues than in those treated with free Pc 4, suggesting the NP-based Pc 4 delivery utilized both the enhanced permeability and retention (EPR) and targeted endocytosis to achieve higher Pc 4 accumulation in tumor cells than that of free Pc 4. To confirm the specific accumulation of NP-based Pc 4 in tumor cells, we also conducted Prussian Blue staining. Figure 5F shows no blue staining in tumors from free Pc 4 treated mice. A greater level of blue staining was found in tumors treated with Fmp-IO-Pc 4 than tumors treated with IO-Pc 4 (Figure 5F).
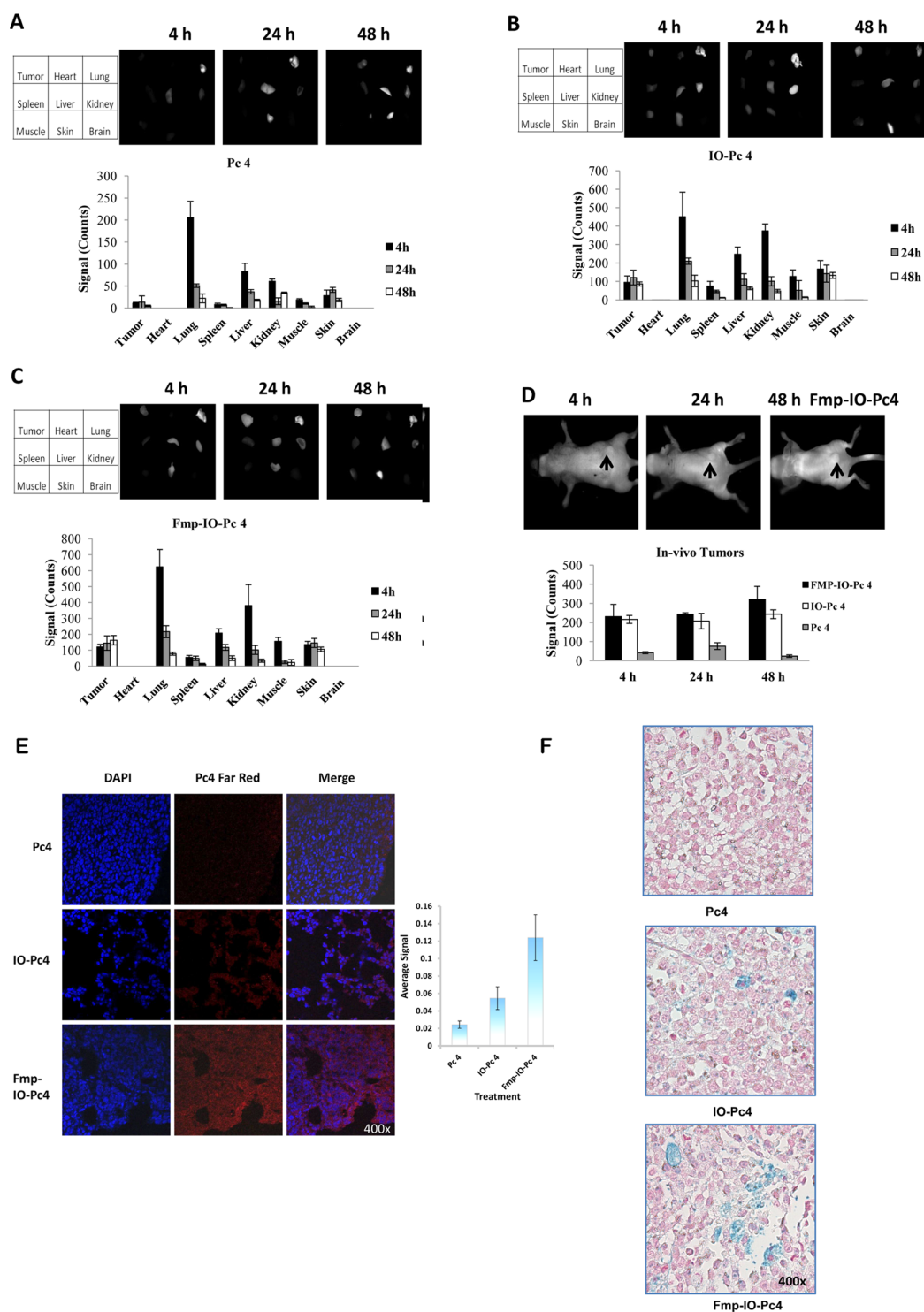
Figure 5. Tissue biodistribution of free Pc 4 and both targeted and nontargeted IO-Pc 4 NPs. Drug distribution studies show that Fmp-IO-Pc 4 has a more prolonged existence in xenografted tumors than free Pc 4 and nontargeted IO-Pc 4. Mice were given Pc 4, IO-Pc 4 or Fmp-IO-Pc 4. Mouse whole-body images and organ images were taken 4, 24, and 48 h after drug administration. (A—C) Images of different organs, including the xenograft tumors, and levels of Pc 4 delivered as free Pc 4, IO-Pc 4 and Fmp-IO-Pc 4 at different time points, respectively (images represent 1 out of 3 mice). (D) Levels of Pc 4 delivered as free Pc 4, IO-Pc 4, and Fmp-IO-Pc 4 in tumors at different time points by whole-body imaging. As shown, the targeted nanoparticle Fmp-IO-Pc 4 has a more prolonged retention in tumors than either free Pc4 or the nontargeted nanoparticle IO-Pc 4. (E) Pc4 staining in fixed tumor tissue from the free Pc 4, IO-Pc 4, and Fmp-IO-Pc 4 groups. 4',6-Diamidino-2-phenylindole (DAPI)was used for nuclear labeling. Greater Pc 4 presence was observed in tumor tissues in Fmp-IO-Pc 4 treated mice than in those treated with IO-Pc 4 or free Pc 4 (images represent 1 out of 3 mice). (F) Tumor sections from 3 mice injected with free Pc 4, IO-Pc 4 and Fmp-IO-Pc 4, respectively. No blue staining was found in tumor cells from free Pc 4 treated mice. Higher numbers of tumor cells with blue staining were observed in tumors from Fmp-IO-Pc4 treated mice than from IO-Pc 4 treated mice.
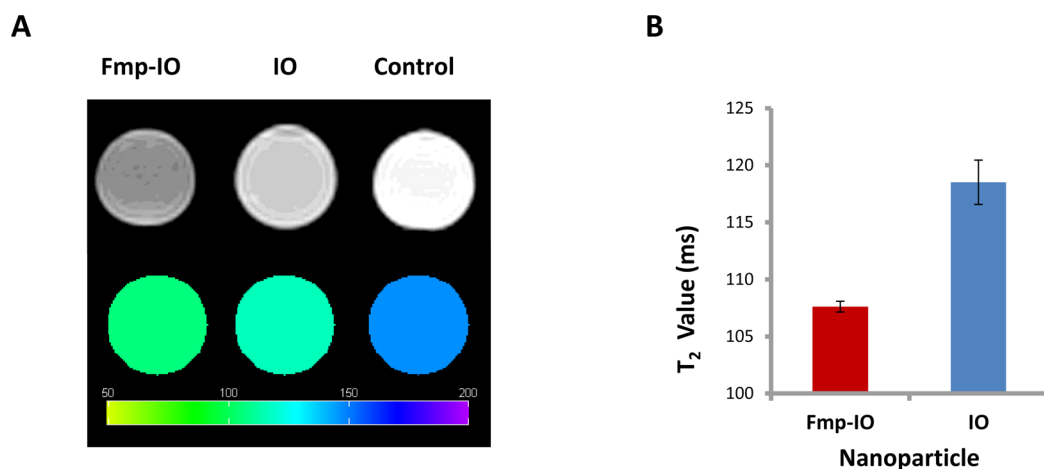
Figure 6. *In vitro* MRI imaging experiment of Fmp-IO-Pc 4. MR imaging and T2 maps of tumor cells incubated with Fmp-IO or IO nanoparticles were collected. (A) shows significant T2 signal decrease in the cells incubated with Fmp-IO as compared to IO nanoparticles or the control without IO. The first well of the upper panel of M4E cells shows a decrease in T2 contrast (darker) for Fmp-IO. The lower panels display the level of T2 values measured by T2 relaxometry mapping method. A low T2 value (green color) correlates with a higher iron concentration, indicating higher level of specific binding of Fmp-IO nanoparticles to tumor cells (image represents 1 out of 3 experiments). Quantitative measures of T2 values show that the cells with Fmp-IO had lower T2 values (107.6 ± 0.47 ms) as compared to those with IO (118.5 ± 1.94 ms) as shown in (B).

Comparison of Effect of Targeted IO Nanoparticle with Non-Targeted IO Nanoparticle on MRI T2 Signal. An *in vitro* MRI study was carried out to determine if specific internalization of the targeted Fmp-IO-Pc 4 into cancer cells results in any MRI contrast change, which would suggest that the synthesized Fmp-IO-Pc 4 can potentially serve as both a nanocarrier and an MR imaging agent. MRI scan showed significant T2 signal decrease in M4E cells incubated with targeted Fmp-IO as compared with nontargeted IO nanoparticles or the control cells without IO. As shown in Figure 6A upper panel, M4E cells incubated with Fmp-IO exhibited a decrease in MRI signals (darker for Fmp-IO). The lower panel displays the T2 values for Fmp-IO, IO, and the control, as measured by T2 relaxometry mapping method. A lower T2 value (green color) correlated with a higher iron concentration, indicating a higher level of specific binding of Fmp-IO nanoparticles to M4E cells. Quantitative measurement of T2 values showed that cells with FMP-IO had lower T2 values (107.6 ± 0.47 ms) as compared to those with IO (118.5 ± 1.94 ms).

DISCUSSION

In head and neck cancer patients, new therapeutic strategies are much needed for the treatment of recurrent tumors given the limitations of conventional therapies. PDT has been demonstrated to be a safe and efficient option in the treatment of various cancers.[8] The first-generation photosensitizing drug Photofrin is US-FDA approved for use in PDT in human cancer patients. Using the FDA-approved drug, preliminary PDT studies in HNSCC show that patients with early stage cancers or early recurrences in the oral cavity and larynx tend to have an excellent response to PDT.[12,13] However, Photofrin has several limitation including

skin burns, short absorption wavelength, and serious side effects.[37] The second-generation PDT agent Pc 4 has advantages over the older generation of PDT drugs because it exhibits shortened patient photosensitivity (good clearance) and has long wavelength absorption, thus it lacks important factors contributing to the limitation of photosensitizers in PDT.[14] The NCI's Drug Decision Network sponsored preclinical toxicity and pharmacokinetics evaluations of Pc 4 and developed a formulation appropriate for its use in humans.[38] There are currently two clinical trials evaluating Pc 4-based PDT, and there has been a sustained, significant effort to move Pc 4-PDT into clinical trials for treating patients.[39]

However, free PDT agents alone are not cancer specific. Since PDT agents distribute in both tumor and normal cells, once laser treatment is given, all cells will be subject to cell toxicity effects of PDT agents. To minimize these nontarget side effects, we have taken advantage of the EPR effect of nanoparticle drugs and also employed Fmp as a targeting agent to specifically increase the biodistribution of PDT agent in cancer cells. Our study demonstrated that Pc 4-PDT delivered by targeted IO NPs is effective in the treatment of head and neck cancer in animal models. We were able to reduce the administered NP Pc 4 dose compared to free Pc 4, while achieving a greater efficacy than that of free Pc 4 due to enhanced tumor tissue accumulation of the PDT agent at the same concentration.

Our initial animal studies demonstrated that both targeted (Fmp-IO-Pc 4) and nontargeted (IO-Pc 4) NPs had greater efficacy than free Pc4, although there was no significant difference in treatment efficacy between IO-Pc 4 and Fmp-IO-Pc 4 (Figure 4A). Since the mice were treated with an equivalent dose of Pc 4

in different formats, the increased efficacy maybe a result of the EPR effect, which is one advantageous characteristic of NP-based drug delivery. This speculation is supported by our biodistribution study which showed that Pc 4 delivered by both IO-Pc 4 and Fmp-IO-Pc 4 was retained up to 48 h in tumor tissue at a 10-fold higher level than that of free Pc 4 (Figure 5B,C vs A). Furthermore, though there was no significant difference in Pc 4 accumulation in tumor tissues between IO-Pc 4 and Fmp-IO-Pc 4 treatment groups, fluorescence imaging of xenograft tumor tissue sections clearly showed higher Pc 4 accumulation in tumor cells after administration of the targeted IO NPs than the nontargeted IO NPs (Figure 5E). We, therefore, performed a second animal experiment in which mice were treated with a lower dose of NP Pc 4. Using 0.06 mg/kg Pc 4, which is 10-fold lower than the commonly used dose for free Pc 4,[21] we found that the targeted Fmp-IO-Pc 4 NP was significantly more potent in PDT than the nontargeted IO-Pc 4 (Figure 4B), suggesting that in addition to taking advantage of EPR effect, the targeted IO NPs could facilitate higher tumor cell accumulation of Pc 4, thus achieving a better treatment efficacy than the nontargeted IO NPs. This indication was also supported by our in vitro binding studies (Figure 3).

Targeted therapy offers the ability to circumvent side effects and improve the efficacy of cancer therapeutic drugs. In head and neck cancer, several molecules have been reported to be efficient targeting ligands.[40,41] We selected integrin β1 as a HNSCC target based on its reportedly high level of expression in this cancer type.[31,42] Our own study also showed that integrin β1 plays a pivotal role in head and neck cancer metastasis.[33] A recent report from Eke et al. demonstrated that integrin β1/FAK/cortactin signaling is essential for human head and neck cancer resistance to radiotherapy. Fmp has been shown to efficiently bind to integrin β1 in several studies.[35,43] Our in vitro binding assay results clearly showed that the Fmp-IO-Pc 4 NP specifically bound to integrin β1-positive cells, while no binding to integrin β1 knock-down cells was observed at 4 °C. These results suggest that Fmp can serve as a reliable targeting ligand for integrin β1-positive head and neck cancer, which is consistent with the findings of other researchers.[44] While the merit of using targeted nanotherapeutics in terms of drug efficacy is still under debate, previous studies by our group and others have consistently shown benefit from the targeted delivery of nanotherapeutic agents.[40,45−47] In our current study, although no difference in therapeutic effect between targeted and nontargeted IO-Pc 4 NPs was observed in the animal study at a dose of 0.4 mg/kg Pc 4, the targeted Fmp-IO-Pc 4 NPs clearly showed a higher accumulation in tumor tissues than the nontargeted IO-Pc 4 NPs in both biodistribution studies in whole body/organs and

Pc4 fluorescence imaging in tumor tissue sections. Since singlet oxygen only exists for a very short time (seconds) and travels a very short distance (nm), only a PDT sensitizer that binds and internalizes into cancer cells can have an optimal cytotoxicitic effect in these cells. In this regard, we expect that targeted delivery of nanotherapeutic PDT can enhance cancer cell damage and reduce nonspecific side-effects in noncancerous cells.

Several publications have shown the delivery of PDT agents by NPs, such as micelle-NPs,[48,49] liposome-NPs,[50] and silica-NPs;[51] however, our IO NPs are unique in potentially providing two functions, MRI and PDT, in one agent. The growing needs in biomedical applications have driven the development of multifunctional nanoparticles that simultaneously provide contrast for different imaging modalities and targeted delivery of drugs.[52] Numerous efforts have been focused on combining imaging and therapeutic agents within the same particle in the past decade.[53,54] The combination of imaging and therapy in the same nanoparticle improves personalized medicine by reducing the inconvenience of separate diagnosis and treatment interventions for patients. Poliquen et al. reported IO NPs as suitable MRI agents with an improved biodistribution.[55] Numerous studies have focused on developing improved IONPs for MRI.[24,56] In the meantime, IONPs have also been demonstrated to provide a safe, reliable nanocarrier for chemotherapeutic drugs.[24,57] IO NPs have unique paramagnetic properties, which generate significant susceptibility effects resulting in strong T_2 and T^*_2 contrast, as well as T_1 effects at very low concentrations.[58−61] In addition, IO NPs have a long blood retention time and are generally biodegradable and are considered to have low toxicity.[62] Their biological safety in humans has been tested, with nontargeted IO NPs currently being used in cancer patients to detect liver tumor lesions or lymph node metastases.[63,64] Recent studies have demonstrated that IO NPs can be internalized by various cell lines, which allows for magnetic labeling of the targeted cells.[65,66] These unique IO NP features are particularly valuable for in vivo tumor imaging and drug delivery. Our in vitro MRI results demonstrated that Fmp-IO not only can specifically internalize into cancer cells as a PDT drug carrier, but also has the potential to serve as an MRI contrast agent.

Finally, although NP have been widely studied in drug and gene delivery, there has been increasing concerns regarding the long-term fate of nanoparticles in biological systems and the associated side effects these agents might have. Carbon nanotubes have been shown to induce DNA damage, oxidative stress, and inflammation.[67,68] Other studies suggest that iron oxide nanoparticles induce ROS formation, which causes disruption of the actin cytoskeleton and alteration of endothelial cell morphology and mechanics.[69] Thus, further studies focusing on the long-term

toxicological aspects of each type of nanoparticle delivery system, including iron oxide nanoparticles, need to be emphasized.

CONCLUSION

We have generated a nanotherapeutic drug combining the integrin β1-specific peptide Fmp as a targeting ligand and IO NP as a carrier to deliver the second-generation PDT drug Pc4 as a cytotoxic agent. Our data indicate that Fmp-IO-Pc 4 NP has clear advantages over the free drug Pc 4 and the nontargeted Fmp-IO-Pc 4 NP in both biodistribution and treatment efficacy. Therefore, it has great potential to provide both improved MRI contrast and enhanced PDT efficacy with reduced nonspecific toxicity for the treatment of head and neck cancer.

EXPERIMENTAL SECTION

Synthesis of Targeted Iron Oxide Nanoparticle-Based Fmp-IO-Pc 4. IO nanoparticles (10 nm) were synthesized by a thermal decomposition method.[70] A polymer encapsulating method was employed to produce water-soluble IO nanoparticles with carboxylic acid group by following previously published protocols.[71−73] Fmp peptide was conjugated to carboxyl functionalized IO nanoparticles with diameter of 10 nm (Ocean Nanotech Cat #SHP10) via 1-ethyl-3-(3-(dimethylamino)propyl) carbodiimide (EDC)/N-hydroxysulfosuccinimide (sulfo-NHS) chemistry using a conjugation kit (Ocean Nanotech Cat # ICK). The molar ratio of Fmp to IO nanoparticles was initially set as 30:1. The Fmp-IO conjugates were washed by ultrafiltration (MWCO: 100 K) with borate buffer (20 mM, pH 7.4). HPLC analysis was carried out on an Agilent 1100 Chemstation with an Agilent Zorbax ODS C18 column (4.6 × 250 mm). A 25 min gradient of acetonitrile−water-trifluoroacetic acid (10:20:0.001, v:v:v) (5 to 65%) in water-trifluoroacetic acid (100:0.1, v:v) at a flow rate of 1.0 mg/mL was used as elution. Standard Fmp (1 mg/mL), Fmp in the conjugation mixture before reaction (0.16 mg/mL) and the supernatant after the conjugation reaction were subjected to HPLC analysis. For drug loading, 1 mg of Pc 4 dissolved in methanol (1 mg/mL) was added to 1 mg (Fe) of Fmp-IO (1 mg (Fe)/ml) dropwise under continuous stirring. The mixture was stirred for another 2 h at room temperature in the dark. Loading was confirmed by running the mixture through a spin column (MWCO: 10K) to check the color of the flowthrough. On the basis of the molar extinction coefficient of Pc 4 (668 nm, 230 000) and 10 nm IO (500 nm, 4 700 000), each IO NP contained an estimated 142.6 molecules of Pc 4.

Cell Culture. The HNSCC cell lines M4E, 686LN, and TU212 were maintained as a monolayer culture in Dulbecco's modified Eagle's medium (DMEM)/F12 medium (1:1) supplemented with 10% fetal bovine serum (FBS) as previously described.[33,74] The integrin β1 knock-down cell line M4E-15 was generated using shRNA as described previously.[33]

SRB Assay. The sulforhodamine B (SRB) assay was used for cell growth determination. Cells were seeded in medium with 50 or 100 nM Pc 4, IO-Pc 4 or Fmp-IO-Pc 4 in a 96-well plate for 24 h. Chemically active Pc 4 was confirmed with singlet oxygen assay using Singlet Oxygen Sensor Green Reagent (Molecular Probes Inc., Eugene OR). Laser treatment was given at 5 mW/cm^2 and 200 mJ/cm^2). Cells were fixed with 10% trichloroacetic acid (Sigma-Aldrich St. Louis, MO) after an additional 24, 48 h of culture. Cells then were washed 5 times with distilled and deionized water. After air drying, 50 μL SRB (Sigma-Aldrich St. Louis, MO) was added to the cells and incubated for 10 min. Cells were then washed with 1% acetic acid 5 times. After air drying, 10 mM Tris solution (pH 10) was added to dissolve the bound dye. Cell growth was assessed by optical density (OD) determination at 510 nm using a microplate reader.

In Vitro Imaging and Quantification for Binding Study. M4E and M4E-15 cells were seeded on Lab-Tek II chamber slide (NalgeNunc International Naperville, IL) with 3000 cells per well. After 24 h, IO-Pc 4 or Fmp-IO-Pc 4 was added at a dose of 100 nM Pc 4. Cells were kept at 4 or 37 °C for 2 h. Cells were then fixed with zinc formalin (Thermo Scientific Kalamazoo, MI) and washed with phosphate-buffered saline (PBS). Pc 4 binding was imaged using Olympus IX71 microscopy with the Nuance Multispectral Image System Nuance 3.1 (Caliper/PerkinElmer

Life Sciences and Technology). After a spectral library was established for the Pc 4 signal and background autofluorescence, a spectral unmixing algorithm was applied to composite images to determine the intensity and location of Pc 4.

Animal Xenograft Model. Animal experiments were approved by the Animal Care and Use Committee of Emory University. Twenty four female nude mice (athymic nu/nu, Taconic, NY, USA) aged 4−6 weeks were injected with 2 × 10^6 M4E cells subcutaneously on both sides. Mice were randomized into 4 groups to ensure similar average tumor size. Pc 4, IO-Pc 4, and Fmp-IO-Pc 4 at the equivalent Pc 4 dose of 0.4 mg/kg body weight were systemically given by I.V. injection when tumor volumes reached 100 mm^3. The control group was injected with saline. Laser illumination was given 48 h after Pc 4 administration. For PDT, the tumor was illuminated for 25 min with light of a 150 J/cm^2 fluence and 100 mW/cm^2 irradiance using a diode laser (Applied Optronics Corp., Newport, CT). The light was delivered with a wavelength of 672 nm at which Pc 4 attains maximal absorption. The light was adjusted to illuminate the whole tumor and spare the surrounding skin which was covered with black tapes to avoid possible damage. Tumor size and body weight were measured every 2 days. Mice were euthanized at day 15. Major organs including lung, liver, heart, spleen and kidney were collected for H&E staining.

A second in vivo experiment employed similar procedures to the first except that the injected dose of Pc 4 was 0.06 mg/kg. In addition, the laser treatment was performed 4 h after the drug administration instead of 48 h.

In Vivo Fluorescence Imaging for Whole Mouse and Organ Biodistribution. Mice bearing xenografted tumor (3 weeks after the cell injection) were imaged using the CRi Maestro imaging device. During imaging acquisitions, the animals were anesthetized with a continuous supply of 2% isofluorane in oxygen. An orange excitation filter (586 nm −601 nm) and a 680 nm long-pass emission filter (640 nm −820 nm) were used to obtain images from 640 to 900 nm in 10 nm wavelength increments. Using the in vivo spectral libraries of Pc 4, IO-Pc 4, Fmp-IO-Pc 4 and the background autofluorescence signals, a spectral unmixing algorithm was applied to composite images to determine the intensity and location of the drugs. The signal at each pixel of a region of interest (ROI) was obtained in a grayscale representation of the unmixed images. The mean signals of the ROIs were calculated and analyzed. To determine whether the difference between these means was statistically significant, an unpaired student's t test was performed. After the whole-body scan, mice were euthanized, organs including lung, heart, brain, liver, spleen, kidney, muscle, skin, and tumors were harvested and were scanned by the multispectral fluorescence imaging system as described above.

Prussian Blue Staining of Tumor Tissue. Frozen sections of xenograft tumors were prepared 48h after drug injection. Sections were fixed with acetone and washed with PBS 3 times. Sections were then incubated at 37 °C for 4 h with 10% (g/mL) of K$_4$Fe(CN)$_6$ in 5%(V/V) HCl (freshly made). Sections were washed with PBS 3 times and stained with Fast Red for 30 min at room temperature.

In Vitro MRI Study. M4E cancer cells (5 × 10^6) were harvested from cell culture after incubating with 10 nM of various IO nanoparticles for 3 h. Cells were washed with phosphate buffer saline (PBS) and then embedded in 1% agarose in multiwell

plates. The cells were then scanned using a 3-T clinical MR scanner (Magnetom Trio, A Tim System, Siemens Medical Solutions USA, Inc., Malvern, PA) and a multiecho T2 weighted fast spin echo imaging sequence to collect a series of echo time (TE) dependent data points simultaneously (15 different TE values ranging from 11 to 165 ms). FMP-IO-induced MRI signal changes in tumor cells were measured in the selected region of interest (ROI). T2 values of each sample were calculated from the captured MRI by fitting the decay curve on a pixel-by-pixel basis using the nonlinear monoexponential algorithm of $M_i = M_0 \times \exp(-TE_i/T2)$.

Statistical Analysis. Student's t test was applied to evaluate the difference between two experimental groups in both *in vitro* binding assays and *in vivo* biodistribution studies. For the *in vivo* efficacy study, the mean longitudinal tumor volumes in the 4 different treatment groups (control, 0.4 mg/kg Pc 4, IO-Pc 4, and Fmp-Io-Pc 4) at different time points within laser treated or nontreated groups were first graphically presented (Figure 4A). The linear mixed model was then used to test (1) whether there is a significant difference in the longitudinal tumor volume between the laser treated and nontreated groups, (2) whether there is any significant difference in tumor volume across the 4 groups within the laser treated and nontreated groups, (3) whether there is any significant growth trend of tumor volume over time, and (4) pairwise group comparison of longitudinal tumor volume within laser treated and nontreated groups. For the second *in vivo* efficacy study, the mean and standard error of the longitudinal tumor volumes of 2 different drug groups (IO-Pc 4 and Fmp-IO-Pc 4) or 2 different treatment groups at different time points within laser treated or nontreated groups were calculated and graphically presented. The generalized estimating equation (GEE) model was employed to test whether there were any significant differences in tumor volume over time across different drug groups and different laser treatment groups. The significance level for data analysis was set at 0.05. SAS 9.3 (SAS Institute, Inc., Cary, NC) was used for data analyses and management.

Conflict of Interest: The authors declare no competing financial interest.

Supporting Information Available: Detail of *in vitro* MRI study, synthesis of targeted iron oxide nanoparticle-based Fmp-IO-Pc 4, Pc 4 dosage and biodistribution. This material is available free of charge *via* the Internet at http://pubs.acs.org.

REFERENCES AND NOTES

1. Siegel, R.; Naishadham, D.; Jemal, A. Cancer Statistics. *Ca—Cancer J. Clin.* **2013**, *63*, 11–30.
2. Jermal, A.; Bray, F.; Center, M. M.; Ferlay, J.; Forman, D. Global Cancer Statistics. *Ca—Cancer J. Clin.* **2011**, *61*, 69–90.
3. Molin, Y.; Fayette, J. Current Chemotherapies for Recurrent/Metastatic Head and Neck Cancer. *Anticancer Drugs* **2011**, *22*, 621–625.
4. Shin, D. M.; Khuri, F. R. Advances in the Management of Recurrent or Metastatic Squamous Cell Carcinoma of the Head and Neck. *Head Neck* **2013**, *35*, 443–453.
5. Dolmans, D. E.; Fukumura, D.; Jain, R. K. Photodynamic Therapy for Cancer. *Nat. Rev. Cancer* **2003**, *3*, 380–387.
6. Hahn, S. M.; Smith, R. P.; Friedberg, J. Photodynamic Therapy for Mesothelioma. *Curr. Treat. Options Oncol.* **2001**, *2*, 375–383.
7. Oleinick, N. L.; Morris, R. L.; Belichenko, I. The Role of Apoptosis in Response to Photodynamic Therapy: What, Where, Why, and How. *Photochem. Photobiol. Sci.* **2002**, *1*, 1–21.
8. Agostinis, P.; Berg, K.; Cengel, K. A.; Foster, T. H.; Girotti, A. W.; Gollnick, S. O.; Hahn, S. M.; Hamblin, M. R.; Juzeniene, A.; Kessel, D.; *et al.* Photodynamic Therapy of Cancer: an Update. *Ca—Cancer J. Clin.* **2011**, *61*, 250–281.
9. Idris, N. M.; Gnanasammandhan, M. K.; Zhang, J.; Ho, P.; Mahendran, R.; Zhang, Y. *In Vivo* Photodynamic Therapy Using Upconversion Nanoparticles as Remote-controlled Nanotransducers. *Nat. Med.* **2012**, *18*, 1580–1585.
10. Civantos, F. Photodynamic Therapy for Head and Neck Lesions in the subtropics. *J. Natl. Compr. Cancer Network* **2012**, *10* (suppl2s), s65–s68.
11. Jerjes, W.; Upile, T.; Hamdoon, Z.; Alexander Mosse, C.; Morcos, M.; Hopper, C. Photodynamic Therapy Outcome for T1/T2 N0 Oral Squamous Cell Carcinoma. *Lasers Surg. Med.* **2011**, *43*, 463–469.
12. Biel, M. A. Photodynamic Therapy of Head and Neck Cancers. *Methods Mol. Biol.* **2010**, *635*, 281–293.
13. Rigual, N. R.; Thankappan, K.; Cooper, M.; Sullivan, M. A.; Dougherty, T.; Popat, S. R.; Loree, T. R.; Biel, M. A.; Henderson, B. Photodynamic Therapy for Head and Neck Dysplasia and Cancer. *Arch. Otolaryngol., Head Neck Surg.* **2009**, *135*, 784–788.
14. He, J.; Larkin, H. E.; Li, Y. S.; Rihter, B. S.; Zaidi, S.; Rodgers, M. A.; Mukhtar, H.; Kenney, M. E.; Oleinick, N. L. The Synthesis, Photophysical and Photobiological Properties and *In Vitro* Structure—Activity Relationships of a Set of Silicon Phthalocyanine PDT Photosensitizers. *Photochem. Photobiol.* **1997**, *65*, 581–586.
15. Baron, E. D.; Malbasa, C. L.; Santo-Domingo, D.; Fu, P.; Miller, J. D.; Hanneman, K. K.; Hsia, A. H.; Oleinick, N. L.; Colussi, V. C.; Cooper, K. D. Silicon Phthalocyanine (Pc 4) Photodynamic Therapy is a Safe Modality for Cutaneous Neoplasms: Results of a Phase 1 Clinical Trial. *Lasers Surg. Med.* **2010**, *42*, 728–735.
16. Lee, T. K.; Baron, E. D.; Foster, T. H. Monitoring Pc 4 Photodynamic Therapy in Clinical Trials of Cutaneous T-Cell Lymphoma Using Noninvasive Spectroscopy. *J. Biomed. Opt.* **2008**, *13*, 030507.
17. Wang, H.; Fei, B. Diffusion-Weighted MRI for Monitoring Tumor Response to Photodynamic Therapy. *J. Magn. Reson. Imaging* **2010**, *32*, 409–417.
18. Fei, B.; Wang, H.; Wu, C.; Chiu, S. M. Choline PET for Monitoring Early Tumor Response to Photodynamic Therapy. *J. Nucl. Med.* **2010**, *51*, 130–138.
19. Fei, B.; Wang, H.; Wu, C.; Meyers, J.; Xue, L. Y.; Maclennan, G.; Schluchter, M. Choline Molecular Imaging with Small-Animal PET for Monitoring Tumor Cellular Response to Photodynamic Therapy of Cancer. *Proc. SPIE* **2009**, *7262*, 1–11.
20. Cheng, Y.; Samia, A. C.; Meyers, J. D.; Panagopoulos, I.; Fei, B.; Burda, C. Highly Efficient Drug Delivery with Gold Nanoparticle Vectors for *In Vivo* Photodynamic Therapy of Cancer. *J. Am. Chem. Soc.* **2008**, *130*, 10643–10647.
21. Fei, B.; Wang, H.; Meyers, J. D.; Feyes, D. K.; Oleinick, N. L.; Duerk, J. L. High-Field Magnetic Resonance Imaging of the Response of Human Prostate Cancer to Pc 4-Based Photodynamic Therapy in an Animal Model. *Lasers Surg. Med.* **2007**, *39*, 723–730.
22. Fei, B.; Wang, H.; Muzic, R. F., Jr.; Flask, C.; Wilson, D. L.; Duerk, J. L.; Feyes, D. K.; Oleinick, N. L. Deformable and Rigid Registration of MRI and MicroPET Images for Photodynamic Therapy of Cancer in Mice. *Med. Phys.* **2006**, *33*, 753–760.
23. Davis, E. D.; Chen, Z. G.; Shin, D. M. Nanoparticle Therapeutics: An Emerging Treatment Modality for Cancer. *Nat. Rev. Drug Discovery* **2008**, *7*, 772–783.
24. Lee, S. J.; Lee, H. J.; Moon, M. J.; Vu-Quang, H.; Lee, H. J.; Muthiah, M.; Che, H. L.; Heo, S. U.; Jeong, H. J.; Jeong, Y. Y.; *et al.* Superparamagnetic Iron Oxide Nanoparticles-Loaded Polymersome-Mediated Gene Delivery Guided by Enhanced Magnetic Resonance Signal. *J. Nanosci. Nanotechnol.* **2011**, *11*, 7057–7060.
25. Hayashi, K.; Nakamura, M.; Sakamoto, W.; Yogo, T.; Miki, H.; Ozaki, S.; Abe, M.; Matsumoto, T.; Ishimura, K. Superparamagnetic Nanoparticle Clusters for Cancer Theranostics

Combining Magnetic Resonance Imaging and Hyperthermia Treatment. *Theranostics* **2013**, *3*, 366–376.

26. Fang, C.; Veiseh, O.; Kievit, F.; Bhattarai, N.; Wang, F.; Stephen, Z.; Li, C.; Lee, D.; Ellenbogen, R. G.; Zhang, M. Functionalization of Iron Oxide Magnetic Nanoparticles with Targeting Ligands: Their Physicochemical Properties and *In Vivo* Behavior. *Nanomedicine (London, U. K.)* **2010**, *5*, 1357–1369.

27. He, H.; David, A.; Chertok, B.; Cole, A.; Lee, K.; Zhang, J.; Wang, J.; Huang, Y.; Yang, V. C. Magnetic Nanoparticles for Tumor Imaging and Therapy: A So-Called Theranostic System. *Pharm. Res.* **2013**, *30*, 2445–2458.

28. Choi, H. S.; Frangioni, J. V. Nanoparticles for Biomedical Imaging: Fundamentals of Clinical Translation. *Mol. Imaging* **2010**, *9*, 291–310.

29. Tassa, C.; Shaw, S. Y.; Weissleder, R. Dextran-Coated Iron Oxide Nanoparticles: A Versatile Platform for Targeted Molecular Imaging, Molecular Diagnostics, and Therapy. *Acc. Chem. Res.* **2011**, *44*, 842–852.

30. Wu, C.; Bauer, J. S.; Juliano, R. L.; McDonald, J. A. The Alpha 5 Beta 1Integrin Fibronectin Receptor, but not the Alpha 5 Cytoplasmic Domain, Functions in an Early and Essential Step in Fibronectin Matrix Assembly. *J. Biol. Chem.* **1993**, *268*, 21883–21888.

31. Van Waes, C.; Surth, D. M.; Chen, Z.; Kirby, M.; Rhim, J. S.; Brager, R.; Sessions, R. B.; Poore, J.; Wolf, G. T.; Carey, T. E. Increase in Suprabasilar Integrin Adhesion Molecule Expression in Human Epidermal Neoplasms Accompanies Increased Proliferation Occurring with Immortalization and Tumor Progression. *Cancer Res.* **1995**, *55*, 5434–5444.

32. Eke, I.; Deuse, Y.; Hehlgans, S.; Gurtner, K.; Krause, M.; Baumann, M.; Shevchenko, A.; Sandfort, V.; Cordes, N. β1 Integrin/FAK/Cortactin Signaling is Essential for Human Head and Neck Cancer Resistance to Radiotherapy. *J. Clin. Invest.* **2012**, *122*, 1529–1540.

33. Wang, D.; Muller, S.; Amin, A. R.; Huang, D.; Su, L.; Hu, Z.; Rahman, M. A.; Koenig, L.; Chen, Z.; Tighiouart, T.; *et al.* The Pivotal Role of Integrinb1 in Metastasis of Head and Neck Squamous Cell Carcinoma. *Clin. Cancer Res.* **2012**, *18*, 4589–4599.

34. Mardilovich, A.; Craig, J. A.; McCammon, M. Q.; Garg, A.; Kokkoli, E. Design of a Novel Fibronectin-Mimetic Peptide-Amphiphile for Functionalized Biomaterials. *Langmuir* **2006**, *22*, 3259–3264.

35. Garg; Kokkoli, E. pH-Sensitive PEGylated Liposomes Functionalized with a Fibronectin-Mimetic Peptide Show Enhanced Intracellular Delivery to Colon Cancer Cell. *Curr. Pharm. Biotechnol.* **2011**, *12*, 1135–1143.

36. Flors, C.; Fryer, M. J.; Waring, J.; Reeder, B.; Bechtold, U.; Mullineaux, P. M.; Nonell, S.; Wilson, M. T.; Baker, N. R. Imaging the Production of Singlet Oxygen *In Vivo* Using A New Fluorescent Sensor, Singlet Oxygen Sensor Green. *J. Exp. Bot.* **2006**, *57*, 1725–1734.

37. Yano, T.; Muto, M.; Minashi, K.; Iwasaki, J.; Kojima, T.; Fuse, N.; Doi, T.; Kaneko, K.; Ohtsu, A. Photodynamic Therapy as Salvage Treatment for Local Failure after Chemoradiotherapy in Patients with Esophageal Squamous Cell Carcinoma: A Phase II Study. *Int. J. Cancer* **2012**, *131*, 1228–1234.

38. Egorin, M. J.; Zuhowski, E. G.; Sentz, D. L.; Dobson, J. M.; Callery, P. S.; Eiseman, J. L. Plasma Pharmacokinetics and Tissue Distribution in CD2F1Mice of Pc4 (NSC 676418), A Silicone Phthalocyanine Photodynamic Sensitizing Agent. *Cancer Chemother. Pharmacol.* **1999**, *44*, 283–294.

39. Miller, J. D.; Baron, E. D.; Scull, H.; Hsia, A.; Berlin, J. C.; McCormick, T.; Colussi, V.; Kenney, M. E.; Cooper, K. D.; Oleinick, N. L. Photodynamic Therapy with the Phthalocyanine Photosensitizer Pc 4: the Case Experience with Preclinical Mechanistic and Early Clinical-Translational Studies. *Toxicol. Appl. Pharmacol.* **2007**, *224*, 290–299.

40. Werner, M. E.; Copper, J. A.; Karve, S.; Cummings, N. D.; Sukumar, R.; Li, C.; Napier, M. E.; Chen, R. C.; Cox, A. D.; Wang, A. Z. Folate-Targeted Polymeric Nanoparticle Formulation of Docetaxel is an Effective Molecularly Targeted Radiosensitizer with Efficacy Dependent on the Timing of Radiotherapy. *ACS Nano* **2011**, *5*, 8990–8998.

41. Master, A. M.; Qi, Y.; Oleinick, N. L.; Gupta, A. S. EGFR-Mediated Intracellular Delivery of Pc 4 Nanoformulation for Targeted Photodynamic Therapy of Cancer: *In Vitro* Studies. *Nanomedicine* **2012**, *8*, 655–664.

42. Li, P.; Zhao, Z.j.; Liu, F. Y.; Sun, L. Y.; Ding, X.; Zhang, W. Z. Chemokine Receptor 7 Regulates Cell Adhesion and Migration *via* Beta1 Integrin in Metastatic Squamous Cell Carcinoma of the Head and Neck. *Oncol. Rep.* **2010**, *24*, 988–995.

43. Atchison, N. A.; Fan, W.; Papas, K. K.; Hering, B. J.; Tsapatsis, M.; Kokkoli, E. Binding of the Fibronectin-Mimetic Peptide, PR_b, to Alpha5Beta1 on Pig Islet Cells Increases Fibronectin Production and Facilitates Internalization of PR_b Functionalized Liposomes. *Langmuir* **2010**, *26*, 14081–14088.

44. Pangburn, T. O.; Georgiou, K.; Bates, F. S.; Kokkoli, E. Targeted Polymersome Delivery of siRNA Induces Cell Death of Breast Cancer Cells Dependent upon Orai3 Protein Expression. *Langmuir* **2012**, *28*, 12816–12830.

45. Beech, J. R.; Shin, S. J.; Smith, J. A.; Kelly, K. A. Mechanisms for Targeted Delivery of Nanoparticles in Cancer. *Curr. Pharm. Des.* **2013**, *19*, 6560–6574.

46. Singh, S.; Sharma, A.; Robertson, G. P. Realizing the Clinical Potential of Cancer Nanotechnology by Minimizing Toxicologic and Targeted Delivery Concerns. *Cancer Res.* **2012**, *72*, 5663–5668.

47. Xu, S.; Olenyuk, B. Z.; Okamoto, C. T.; Hamm-Alvarez, S. F. Targeting Receptor-Mediated Endocytotic Pathways with Nanoparticles: Rationale and Advances. *Adv. Drug Delivery Rev.* **2013**, *65*, 121–138.

48. Master, A. M.; Livingston, M.; Oleinick, N. L.; Sen Gupta, A. Optimization of a Nanomedicine-Based Silicon Phthalocyanine 4 Photodynamic Therapy (Pc 4-PDT) Strategy for Targeted Treatment of EGFR-Overexpressing Cancers. *Mol. Pharm.* **2012**, *9*, 2331–2338.

49. Master, A.; Malamas, A.; Solanki, R.; Clausen, D. M.; Eiseman, J. L.; Sen Gupta, A. A Cell-Targeted Photodynamic Nanomedicine Strategy for Head and Neck Cancers. *Mol. Pharm.* **2013**, *10*, 1988–1997.

50. Mir, Y.; Elrington, S. A.; Hasan, T. A New Nanoconstruct for Epidermal Growth Factor Receptor-Targeted Photo-Immunotherapy of Ovarian Cancer. *Nanomedicine* **2013**, *9*, 1114–1122.

51. Li, W.; Lu, W.; Fan, Z.; Zhu, X.; Reed, A.; Newton, B.; Zhang, Y.; Courtney, S.; Tiyyagura, P. T.; Li, S.; *et al.* Enhanced Photodynamic Selectivity of Nano-Silica-Attached Porphyrins Against Breast Cancer Cells. *J. Mater. Chem.* **2012**, *22*, 12701–12708.

52. Bao, G.; Mitragotri, S.; Tong, S. Multifunctional Nanoparticles for Drug Delivery and Molecular Imaging. *Annu. Rev. Biomed. Eng.* **2013**, *15*, 253–282.

53. Le Duc, G.; Miladi, I.; Alric, C.; Mowat, P.; Bräuer-Krisch, E.; Bouchet, A.; Khalil, E.; Billotey, C.; Janier, M.; Lux, F.; *et al.* Toward an Image-Guided Microbeam Radiation Therapy Using Gadolinium-Based Nanoparticles. *ACS Nano* **2011**, *5*, 9566–9574.

54. Yu, M. K.; Kim, D.; Lee, I. H.; So, J. S.; Jeong, Y. Y.; Jon, S. Image-Guided Prostate Cancer Therapy Using Aptamer-Functionalized Thermally Cross-Linked Superparamagnetic Iron Oxide Nanoparticles. *Small* **2011**, *7*, 2241–2249.

55. Pouliquen, D.; Perdrisot, R.; Ermias, A.; Akoka, S.; Jallet, P.; Le Jeune, J. J. Superparamagnetic Iron Oxide Nanoparticles as a Liver MRI Contrast Agent: Contribution of Microencapsulation to Improved Biodistribution. *Magn. Reson. Imaging* **1989**, *7*, 619–627.

56. Kumar, M.; Yigit, M.; Dai, G.; Moore, A.; Medarova, Z. Image-Guided Breast Tumor Therapy Using a Small Interfering RNA Nanodrug. *Cancer Res.* **2010**, *70*, 7553–7561.

57. Ling, D.; Hyeon, T. Iron Oxide Nanoparticles: Chemical Design of Biocompatible Iron Oxide Nanoparticles for Medical Applications. *Small* **2013**, *9*, 1450–1466.

58. Sjogren, C. E.; Johansson, C.; Naevestad, A.; Sontum, P. C.; Briley-Saebo, K.; Fahlvik, A. K. Crystal Size and Properties of Superparamagnetic Iron Oxide (SPIO) Particles. *Magn. Reson. Imaging* **1997**, *15*, 55–67.

59. Wunderbaldinger, P.; Josephson, L.; Bremer, C.; Moore, A.; Weissleder, R. Detection of Lymph Node Metastases by Contrast-Enhanced MRI in an Experimental Model. *Magn. Reson. Med.* **2002**, *47*, 292–297.

60. Hogemann, D.; Josephson, L.; Weissleder, R.; Basilion, J. P. Improvement of MRI Probes to Allow Efficient Detection of Gene Expression. *Bioconjugate Chem.* **2000**, *11*, 941–946.

61. Bulte, J. W.; Kraitchman, D. L. Iron Oxide MR Contrast Agents for Molecular and Cellular Imaging. *NMR Biomed.* **2004**, *17*, 484–99.

62. Moore, A.; Weissleder, R.; Bogdanov, A., Jr. Uptake of Dextran-Coated Monocrystalline Iron Oxides in Tumor Cells and Macrophages. *J. Magn. Reson. Imaging* **1997**, *7*, 1140–1145.

63. Schultz, J. F.; Bell, J. D.; Goldstein, R. M.; Kuhn, J. A.; McCarty, T. M. Hepatic Tumor Imaging Using Iron Oxide MRI: Comparison with Computed Tomography, Clinical Impact, and Cost Analysis. *Ann. Surg. Oncol.* **1999**, *6*, 691–698.

64. Harisinghani, M. G.; Barentsz, J.; Hahn, P. F.; Deserno, W. M.; Tabatabaei, S.; van de Kaa, C. H.; de la Rosette, J.; Weissleder, R. Noninvasive Detection of Clinically Occult Lymph-Node Metastases in Prostate Cancer. *N. Engl. J. Med.* **2003**, *348*, 2491–2499.

65. Kircher, M. F.; Allport, J. R.; Graves, E. E.; Love, V.; Josephson, L.; Lichtman, A. H.; Weissleder, R. *In Vivo* High Resolution Three-Dimensional Imaging of Antigen-Specific Cytotoxic T-Lymphocyte Trafficking to Tumors. *Cancer Res.* **2003**, *63*, 6838–6846.

66. Lewin, M.; Carlesso, N.; Tung, C. H.; Tang, X. W.; Cory, D.; Scadden, D. T.; Weissleder, R. Tat Peptide-Derivatized Magnetic Nanoparticles Allow *In Vivo* Tracking and Recovery of Progenitor Cells. *Nat. Biotechnol.* **2000**, *18*, 410–414.

67. Tang, M. F.; Lei, L.; Guo, S. R.; Huang, W. L. Recent Progress in Nanotechnology for Cancer Therapy. *Chin. J. Cancer* **2010**, *29*, 775–780.

68. Yamashita, K.; Yoshioka, Y.; Kayamuro, H.; Yoshida, T.; Higashisaka, K.; Abe, Y.; Yoshikawa, T.; Itoh, N.; Tsunoda, S.; Tsutsumi, Y. Cancer Hazard of Carbon Nanotubes: Size/Shape-Dependent Induction of DNA Damage and Inflammation. *Cytokine* **2009**, *48*, 55–55.

69. Buyukhatipoglu, K.; Clyne, A. M. Superparamagnetic Iron Oxide Nanoparticles Change Endothelial Cell Morphology and Mechanics *via* Reactive Oxygen Species Formation. *J. Biomed. Mater. Res., Part A* **2011**, *96*, 186–195.

70. Gilli, G.; Schiliro, T.; Traversi, D.; Pignata, C.; Cordara, S.; Carraro, E. Formaldehyde Adduct to Human Serum Albumin with Reference to Aspartame Intake. *Environ. Toxicol. Pharmacol.* **2008**, *25*, 89–93.

71. Higai, K.; Satake, M.; Nishioka, H.; Azuma, Y.; Matsumoto, K. Glycated Human Serum Albumin Enhances Macrophage Inflammatory Protein-1Beta mRNA Expression through Protein Kinase C-Delta and NADPH Oxidase in Macrophage-Like Differentiated U937 Cells. *Biochim. Biophys. Acta* **2008**, *1780*, 307–314.

72. Katavetin, P.; Inagi, R.; Miyata, T.; Tanaka, T.; Sassa, R.; Ingelfinger, J. R.; Fujita, T.; Nangaku, M. Albumin Suppresses Vascular Endothelial Growth Factor *via* Alteration of Hypoxia-Inducible Factor/Hypoxia-Responsive Element Pathway. *Biochem. Biophys. Res. Commun.* **2008**, *367*, 305–310.

73. Yokoe, J.; Sakuragi, S.; Yamamoto, K.; Teragaki, T.; Ogawara, K.; Higaki, K.; Katayama, N.; Kai, T.; Sato, M.; Kimura, T. Albumin-Conjugated PEG Liposome Enhances Tumor Distribution of Liposomal Doxorubicin in Rats. *Int. J. Pharm.* **2008**, *353*, 28–34.

74. Wang, D.; Su, L.; Huang, D.; Zhang, H.; Shin, D. M.; Chen, Z. G. Downregulation of E-Cadherin Enhances Proliferation of Head and Neck Cancer through Transcriptional Regulation of EGFR. *Mol. Cancer* **2011**, *10*, 116.